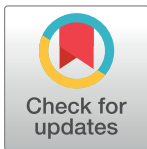RESEARCH ARTICLE

Lateral frontoparietal effective connectivity differentiates and predicts state of consciousness in a cohort of patients with traumatic disorders of consciousness

Riku Ihalainen[1,2], Jitka Annen[3,4,5], Olivia Gosseries[3,4], Paolo Cardone[3,4], Rajanikant Panda[3,4], Charlotte Martial[3,4], Aurore Thibaut[3,4], Steven Laureys[3,6,7], Srivas Chennu[2]* *

1 Department of Anesthesia, Critical Care and Pain Medicine, Beth Israel Deaconess Medical Center, Boston, MA, United States of America, **2** School of Computing, University of Kent, Canterbury, United Kingdom, **3** Coma Science Group, GIGA Consciousness Research Unit, University and University Hospital of Liège, Liège, Belgium, **4** Centre du Cerveau[2], University Hospital of Liège, Liège, Belgium, **5** Department of Data Analysis, University of Ghent, Ghent, Belgium, **6** CERVO Brain Research Centre, de la Canardière, Québec, Canada, **7** Consciousness Science Institute, Hangzhou Normal University, Hangzhou, Zhejiang, China

☯ These authors contributed equally to this work.
* sc785@kent.ac.uk

Abstract

Neuroimaging studies have suggested an important role for the default mode network (DMN) in disorders of consciousness (DoC). However, the extent to which DMN connectivity can discriminate DoC states–unresponsive wakefulness syndrome (UWS) and minimally conscious state (MCS)–is less evident. Particularly, it is unclear whether effective DMN connectivity, as measured indirectly with dynamic causal modelling (DCM) of resting EEG can disentangle UWS from healthy controls and from patients considered conscious (MCS+). Crucially, this extends to UWS patients with potentially "covert" awareness (minimally conscious star, MCS*) indexed by voluntary brain activity in conjunction with partially preserved frontoparietal metabolism as measured with positron emission tomography (PET+ diagnosis; in contrast to PET- diagnosis with complete frontoparietal hypometabolism). Here, we address this gap by using DCM of EEG data acquired from patients with traumatic brain injury in 11 UWS (6 PET- and 5 PET+) and in 12 MCS+ (11 PET+ and 1 PET-), alongside with 11 healthy controls. We provide evidence for a key difference in left frontoparietal connectivity when contrasting UWS PET- with MCS+ patients and healthy controls. Next, in a leave-one-subject-out cross-validation, we tested the classification performance of the DCM models demonstrating that connectivity between medial prefrontal and left parietal sources reliably discriminates UWS PET- from MCS+ patients and controls. Finally, we illustrate that these models generalize to an unseen dataset: models trained to discriminate UWS PET- from MCS+ and controls, classify MCS* patients as conscious subjects with high posterior probability (pp > .92). These results identify specific alterations in the DMN after severe brain injury and highlight the clinical utility of EEG-based effective connectivity for identifying patients with potential covert awareness.

Introduction

After a severe brain injury, patients may be diagnosed with a transient or permanent disorders of consciousness (DoC), such as the unresponsive wakefulness syndrome (UWS) or the minimally conscious state (MCS). The UWS is defined by preserved arousal in the absence of behavioral signs of awareness (periodic sustained eye opening with purposeless movements) [1]. In contrast, patients in MCS show fluctuating but reproducible signs of consciousness with preserved arousal. The MCS has been further divided into MCS- and MCS+, with the latter condition characterized by command following, intelligible verbalization, or gestural or verbal yes/no responses (regardless of accuracy) to spoken or written questions [2].

The exclusive use of clinical consensus for diagnosing these DoC based on observed behaviors has been shown to result in high rates of misdiagnosis of the accurate level of consciousness of the DoC patients, especially in the case of patients suffering from UWS [3–5]. Consequently, with the advent of modern neuroimaging techniques, there has been increasing interest in characterizing the underlying neuronal basis for the presence or lack of awareness in DoC using structural and functional magnetic resonance imaging (MRI/fMRI; [6, 7]), positron emission tomography (PET; [3, 8]), and electroencephalography (EEG; e.g., [9–11]).

Structural and functional neuroimaging studies have suggested an important role of the default mode network (DMN) in DoC–an intrinsic brain network encompassing the posterior cingulate cortex/precuneus, bilateral parietal cortices, and the medial prefrontal cortex [12–17]. In parallel, cerebral metabolism as measured by PET has been shown to differentiate UWS from MCS [4, 18], with regional differences often in areas associated with DMN [19, 20]. This extends to patients with MCS; MCS+ can be distinguished from MCS- with the former group showing partially preserved language related behaviors (e.g., response to simple commands) alongside with a higher cerebral metabolism especially in left-sided cortical areas, including Broca's and Wernicke's areas, premotor, presupplementary motor, and sensorimotor cortices [21–23]. A trained neurologist can diagnose patients also based on a visual inspection of their underlying PET metabolism, to as either PET negative (-) or PET positive (+). A PET- diagnosis is typically produced by a complete bilateral hypometabolism of the associative frontoparietal cortex with no voxels with preserved metabolism, whereas PET+ diagnosis is characterized by an incomplete hypometabolism and partial preservation of activity within these areas [3, 21, 24].

In addition, effective connectivity studies in DoC as measured with dynamic causal modelling (DCM) for fMRI have suggested disruptions within the DMN specifically related to posterior cingulate cortex (PCC) [25] and in subcortical networks, potentially driving the disruptions in the DMN [26, 27]. DCM is a generic approach used to infer hidden (or unobserved) neuronal states from measured brain activity; the idea is to model the source activity over time in terms of causal relationships between interacting inhibitory and excitatory populations of neurons. As far as we know, only one study has used DCM with EEG for measuring and diagnosing cognitive functioning in DoC population. Using a mismatch negativity paradigm, Boly and colleagues [28] showed that the difference between UWS and MCS was due to an impairment of backward connectivity from frontal to temporal cortices, emphasizing the importance of top-down processing for conscious perception.

Importantly, a number of studies have suggested residual consciousness and/or reported "covert" voluntary brain activity in some seemingly unresponsive patients, with both, active and resting state paradigms [29–37]. These patients, who show no behavioral signs of consciousness, yet with whose neuroimaging results indicate residual brain activity compatible with the diagnosis of MCS, have been termed MCS* (minimally conscious state star) [4, 38]. To keep consistent with the literature, from this point on, we use the term MCS* to refer to the UWS patients with PET+ diagnosis in this manuscript.

Currently it is unknown whether effective resting state connectivity between key nodes within the DMN, as measured with EEG, could be used to identify such covertly aware patients. Here, as a preliminary investigation, we address this gap by using spectral DCM for EEG with parametric empirical Bayes (PEB). We investigate the difference in causal interactions between cortico-cortical regions of the DMN, between DoC patients (UWS and MCS+) and healthy controls. First, our interest is in distinguishing the differences between UWS patients and healthy controls, and in demonstrating the prospective performance of the connectivity within DMN in classifying these states. Crucially, we include MCS+ patients to function as a second, yet demonstrably conscious, control group to reduce the probability that our findings reflect mainly damage in the brain, and not consciousness itself. Based on previous studies [28], we hypothesize that there will be top-down/backward connectivity differences in UWS vs. healthy controls and in UWS vs. MCS+ comparisons. We also model the difference between MCS+ and healthy controls where we do not expect to see this difference.

Next, in a leave-one-subject-out cross-validation, we test the classification performance of models based on the fully connected DMN network and on two connectivity subsets of the DMN: the posterior connections and the frontoparietal connections. Following this, we adopt a data-driven approach to the classification problem by investigating the predictive performance of single connections. The aim here is to identify the direction and location of the largest, most consistent modulations between the subjects.

Finally, we demonstrate that our DCM models generalize to a more difficult classification problem: in a leave-one-*state*-out cross-validation paradigm, we train the models on UWS patients with a confirmed PET negative (PET-) diagnosis (i.e., a complete bilateral hypometabolism of the associative frontoparietal cortex) on the one hand and either healthy controls or MCS+ patients on the other. The MCS+ patients here function as a conscious control group who still suffer from brain damage. We then test the models on datasets from "covertly aware" MCS* patients (partially preserved metabolism and activity within these areas). We hypothesize that if our modelled effects are valid, and if the sustained PET metabolism reflects covert awareness in the MCS* patients, our model should classify these patients as healthy controls/MCS+ rather than UWS PET-.

Methods

Data acquisition

We assessed effective connectivity within the DMN and whether modulation of this connectivity predicted states of consciousness in patients with DoC. The patients included were referred to the University and University Hospital of Liège (Coma Science Group and Centre du Cerveau[2]) from clinical centers across Europe since 2008. The data collection was approved by the Ethics Committee of the University Hospital of Liège and the patients' legal guardians gave written informed consent. Data were also collected from healthy controls as a reference group, all of whom gave informed written consent before participation. For the present study, anonymized data were obtained in September 2017.

The dataset consisted of the patient data with 26 healthy controls (total $N = 188$). Parts of these data have already been published in previous studies [31, 39, 40]. From the dataset, we identified patients admitted due to traumatic brain injury (TBI; $N = 76$). Amongst the TBI patients, we further identified those diagnosed with UWS ($N = 11$) [1] or MCS+ ($N = 12$) [2]. Patients admitted due to any other etiology, e.g., anoxia or hemorrhage, and patients diagnosed with any other condition than UWS or MCS+, were excluded from the further analyses. See S1 Text for more details of the rationale and process of pruning the dataset, and for S2 Table in S1 Text of UWS and MCS+ patients' clinical characteristics. The patient groups were

Table 1. Cohort background data. The mean age in years (SD), the total number of patients (females), the number of PET+ and PET- patients, and the time since onset of injury in each of the different DoC-groups. UWS–unresponsive wakefulness syndrome, MCS+–minimally conscious state plus, TBI–traumatic brain injury.

Patient group	Mean age (SD) in years	N^{TOTAL} (females)	PET+	PET-	Etiology	Mean time since injury (days)
UWS	30.7 (8.5)	11 (4)	5	6	TBI	599
MCS+	38.3 (10.3)	12 (3)	11	1	TBI	1033
Controls	30.9 (6.7)	11 (4)	-	-	-	-

further divided based on their respective PET-scans–either into a PET positive (PET+) or a PET negative (PET-) sub-group (Table 1). Amongst the healthy controls, using the random number generator in MATLAB, we (pseudo-randomly) drew a cohort of 11 control subjects to adjust for the group-size discrepancies. There were no meaningful differences in the mean ages nor in mean days since injury between the groups (in a Bayesian ANOVA the probability for the model including the main effect of age: p(M|data) = 0.247, Bayes factor = 0.328, main effect of time since injury: p(M|data) = 0.260, Bayes factor = 0.351). Female/male ratios were 0.36 for UWS, 0.25 for MCS+ and 0.36 for controls.

Both PET scans and high-density EEG recordings were acquired at the same time and the patients were behaviorally assessed by a trained clinician using the Coma Recovery Scale–Revised (CRS-R) [41] on the same day, before and after the scans (and on other days for at least five assessments). Both patients and healthy volunteers were asked to stay awake during the data collection. The behaviorally apparent arousal levels of patients were monitored during the data collection session to ensure that they stayed awake and awaken with auditory/tactile stimulations if necessary.

PET scans were acquired and interpreted using methodology described in [3] and in the S1 Text. Briefly, the analysis results were visually inspected by a trained clinician/researcher. Complete bilateral hypometabolism of the associative frontoparietal cortex without any voxels with preserved metabolism led to PET- diagnosis, whereas partial preservation with incomplete hypometabolism in these areas yielded a diagnosis of PET+ [20, 24, 42].

The EEG data consisted of high-density EEG recordings of 20–30 minutes (256-channels, EGI), acquired during the F-fluorodeoxyglucose (FDG) uptake, just prior to the start of the PET imaging. The data were recorded at a sampling rate of either 250 Hz or 500 Hz (down-sampled to 250 Hz). Data from the channels from the neck, cheeks, and forehead were discarded due to contributing most of the movement-related noise. We were left with the data from 173 channels on the scalp for further analysis. These 173 electrodes were co-registered to a template MRI mesh in MNI coordinates, and the volume conduction model of the head was based on the Boundary Element Method (BEM). The raw signals were filtered from 0.5–45 Hz, with additional line noise removal at 50 Hz (notch-filter). We further restricted the DCM analysis to 1–30 Hz due to excessive high-frequency noise components. Via calculating the normalized variance, the excessively noisy channels and epochs were identified and either manually rejected or retained by visual inspection. Lastly, the data were re-referenced to a common average.

Dynamic causal modeling

We first imported the first 60 artefact-free 10-second epochs, in to SPM12 (Wellcome Trust Centre for Human Neuroimaging; www.fil.ion.ucl.ac.uk/spm/software/spm12). To analyze the resting effective connectivity within the DMN, DCM for EEG cross-spectral densities (CSD) was applied [43, 44]. Here, the observed cross-spectral densities in the resting-EEG are explained by a generative model that combines a biologically plausible neural mass model with

an electrophysiological forward model mapping the underlying neural states to the observed data (ERP-model; [45]. The idea is to model the source activity over time in terms of causal relationships between interacting inhibitory and excitatory populations of neurons.

Each source–or node–is connected to each other via extrinsic connections, while each sub-population within each source is connected to each other via intrinsic connections. Here, how-ever, we aimed to model disrupted consciousness at the level of active networks, and hence, we estimated extrinsic connectvity between the nodes within the DMN. Among the extrinsic con-nectivity, the top-down–or backward–connections are thought to have inhibitory and modula-tory effects on the nodes they target, while forward connections are viewed as having a strong excitatory driving effect (bottom-up; [46, 47].

Within each node, second-order differential equations describe the hidden state of neural activity that depends on both the parameterized intrinsic and extrinsic connection strengths. This enables the computation of the linear mapping from the endogenous neuronal fluctua-tions to the EEG sensor spectral densities, and consequently, permits the modelling of differ-ences in the spectra due to changes in the underlying neurophysiologically meaningful parameters. These parameters describe, for example, the intrinsic and extrinsic connectivity of coupled neuronal populations (i.e., sources) and their physiology. For further information about EEG DCM, see for example [43, 44, 48].

Model specification

Fitting an EEG DCM model requires the specification of the anatomical locations of the nodes/ sources a priori. Here, the network architecture we model is based on the DMN, which has been previously associated with DoC [25, 49–51]. To that end, we assume four sources, mod-elled as a patch on the cortical surface ('IMG' option in SPM12). The schematic representation and the node locations (adopted from [52]) are shown in Fig 1A and 1B, respectively (node locations visualized with the BrainNet Viewer, [53], http://www.nitrc.org/projects/bnv/). The MNI coordinates are listed in Table 2. We modelled the data using the default DCM settings, standard MNI coordinates for the electrodes, and the forward model provided by SPM12. In the S2 Fig in S1 Text, the mean model fits across the participants are shown, indicating that the DCM fit well the observed CSD's. As shown in Fig 1A, the nodes in the DMN were connected via forward, backward, and lateral connections as described in [54, 55]. Thus, each node was
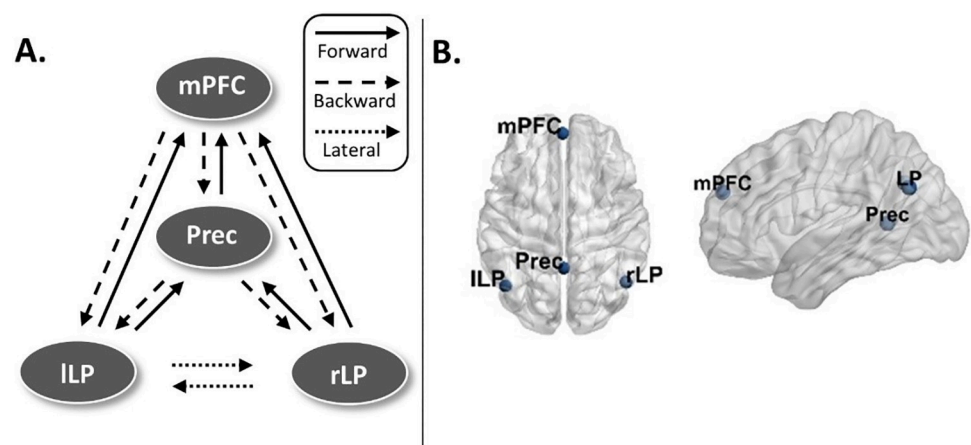
Fig 1. Model specification for the default mode network (DMN). A. The fully connected, schematic representation of the default mode network (DMN). **B.** The node locations for the DMN. mPFC–medial prefrontal cortex, Prec–posterior cingulate cortex/precuneus, lLP–left lateral parietal cortex, rLP–right lateral parietal cortex.

https://doi.org/10.1371/journal.pone.0298110.g001

Table 2. The default mode network nodes and their corresponding MNI coordinates (adapted from [52]).

Network	Coordinates (in mm)		
	x	y	z
Default Mode Network			
Left lateral parietal	-46	-66	30
Right lateral parietal	49	-63	33
Posterior cingulate/precuneus	0	-52	7
Medial prefrontal	-1	54	27

https://doi.org/10.1371/journal.pone.0298110.t002

modelled as a point source with the neuronal activity being controlled by operations following the Jansen-Rit model [56]. These three different types of connections in each model were specified in what is referred in the DCM literature as the 'A-matrix'. This fully connected model was then estimated for each subject using the DCM for CSD [43, 44]; see S1 Text for details.

Parametric empirical Bayes

In DCM, the posterior density over the parameters given by the model inversion process is approximated via a variational Bayesian scheme by maximizing a lower bound (the negative free energy) on the log-evidence (Variational Laplace; [57]. A more recent addition, the PEB framework, can be utilized to infer, for example, the group-level commonalities and differences [58].
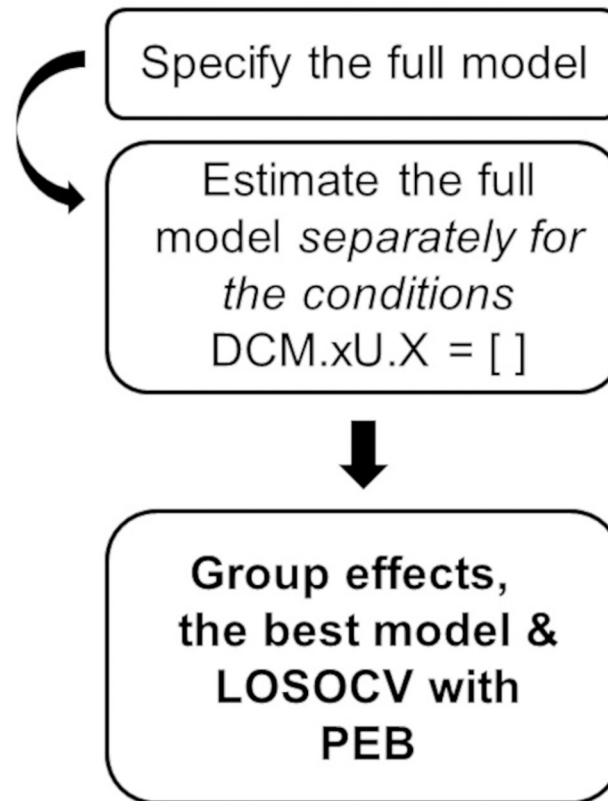
In PEB, the subject-specific parameters–here, the effective connectivity modulations between nodes in DMN–are taken to the group-level and modelled using a General Linear Model (GLM). In doing so, PEB partitions the between-subject variability into designed effects and unexplained random effects (captured by the covariance component). As a special case of Bayesian model selection (BMS), Bayesian model reduction (BMR; [58] enables the inversion of multiple nested models from a single, fully connected ('full') model in a hierarchical manner. In doing so it enables a greedy search to compare the negative free energies for the nested models (reduced models), iteratively discarding the parameters that do not contribute to the free energy (originally 'post-hoc DCM analysis'; [59, 60]. Consequently, PEB conveys both the estimated group-level connection strengths and their respective uncertainty (posterior covariance component). As such, it is argued that hypotheses about commonalities and differences across subjects can be tested with more precise parameter estimates than with traditional frequentist comparisons [58].

A Bayesian Model Average (BMA) is calculated over the best 256 models weighted by their Model evidence; for every connection, a posterior probability for the connection being present vs. absent is calculated by comparing evidence from all the models in which the parameter is switched on vs. all the models in which it is switched off. Here, we applied a threshold of >.99 posterior probability, in other words, connections with over .99 posterior probability were retained. The overall process is shown in Fig 2.

Leave-one-out cross-validation

To validate our modelling framework, we investigated which DMN connections are predictive of the subject group by adapting a standard approach in computational statistics, leave-one-subject-out cross-validation (LOSOCV; spm_dcm_loo.m). Here, we iteratively fitted a multivariate linear model (as described in detail in [58]) to provide the posterior predictive density over connectivity changes, which was then used to evaluate the posterior belief of the

Model fitting pipeline for LOSOCV

Specify the full model

Estimate the full model *separately for the conditions*
DCM.xU.X = [ ]

Group effects, the best model & LOSOCV with PEB

Fig 2. The pipeline for inverting the dynamic causal modelling (DCM) model for different subject-groups. This was done to find the best models for each patient group, to estimate the effective connectivity modulations between the patient groups, and as a prerequisite for the leave-one-subject-out cross-validation (LOSOCV) classification with parametric empirical Bayes (PEB) modelling.

https://doi.org/10.1371/journal.pone.0298110.g002

explanatory variable for the left-out participant: in the present case, the probability of the subject group membership.

To cross-validate a fitted DCM model, one participant was left out each time *before* conducting PEB analysis on the training dataset, and the optimized empirical priors were then used to predict the subject-group to which the dataset from the left-out participant belonged (see [58] for details). We repeated this procedure for each participant, and in doing so generated probabilities of state affiliation (here, posterior probabilities for subject group-membership).

It is worthwhile to note, that we have estimated the DCM models using the default parameter settings recommended in the literature [43, 61, 62]. This is also true for the LOSOCV procedure: no hyper parameter optimization was done. Here, we trained the model with the data from all but the left-out participant (training set), and predicted the state based on the data from the left-out participant (test set) and repeated this procedure leaving out a different participant each time.
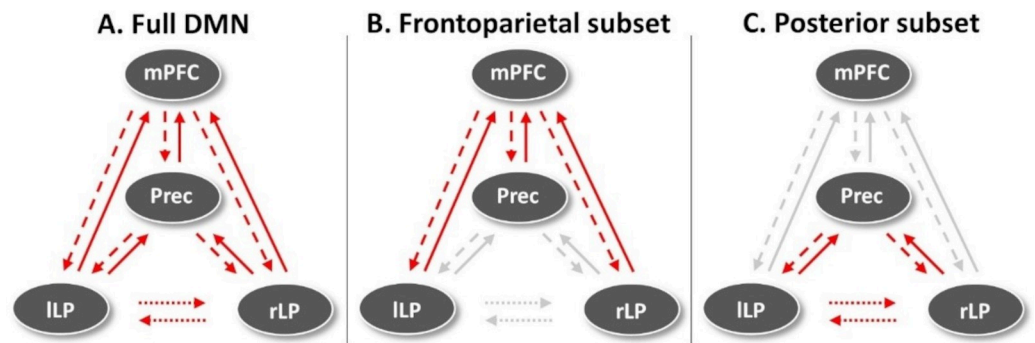
Fig 3. The hypothesis-driven subsets for the LOSOCV-paradigm. The red arrows indicate the connections included in each subset, and the grey arrows the left-out connections. First, predictions based on all connections were estimated (A). Next, predictions based on two connection subsets–frontoparietal (B) and parietal subsets (C)–were estimated. Lastly, we estimated predictions based on single connections in a data-driven approach. mPFC–medial prefrontal cortex, Prec–posterior cingulate cortex/precuneus, lLP–left lateral parietal cortex, rLP–right lateral parietal cortex, DMN–default mode network.

Leave-one-subject-out cross-validation

We first estimated predictive performance in a leave-one-subject-out cross-validation paradigm in which LOSOCV metrics for all connections in the DMN and for a hypothesis-driven subsets were estimated (frontoparietal and parietal subsets; Fig 3). Next, a data-driven approach was used in which we started the estimation from the connection associated with the largest connectivity reduction between the subject-groups and repeated the procedure for all connections. Here, we utilized a forward stepwise regression in which we started the estimation from the connections with the largest changes and continued through the parameters based on their respective modulation effect sizes. Lastly, we combined connections into data-driven subsets, starting from the connections with the best classification performance, until the classification accuracy stopped improving. The rationale was to investigate the location and direction of the most consistent inter-subject-level effects, in addition to the largest effect sizes identified by the PEB analysis.

Leave-one-state-out cross-validation

Finally, the validation process was generalized by introducing two more difficult classification problems: first, we trained the model on the DCM parameters from the control and the UWS PET- groups, and then tested it on unseen data collected from the MCS* patient-group. Second, we trained the model on the data from the MCS+ and the UWS PET- groups, and again tested on the MCS* datasets. Here, the model was trained on all training datasets. As above, the model used the optimized empirical priors to predict the more likely patient-group the test dataset (MCS*) belonged. We hypothesized that if our modelled effects are valid, and if the sustained PET-metabolism reflects higher level of consciousness present in the MCS* patients in comparison to UWS PET- patients, in the former case the model should classify the test datasets as controls rather than UWS PET-. Similarly, in the latter case, given that the MCS+ patients are conscious, the test data should be classified as MCS+ rather than UWS PET-. Here, we used posterior probability for subject group-membership to quantify classification performance.

Results

Dynamic causal modeling and parametric empirical Bayes

Our first goal was to investigate the effective connectivity modulations best explaining the difference between healthy controls, UWS PET-, and MCS+ patients. We modelled time-series

recorded from the three groups with DCM for cross-spectral densities (CSD; [43, 44] at a single-subject level, followed by PEB at the group-level. In doing so, we estimated the change in effective connectivity in 12 inter-node connections in the DMN, contrasting 11 healthy controls both with 6 UWS PET- patients and with 12 MCS+ patients, and the 12 MCS+ patients with 6 UWS PET- patients.

Following the inversion of the between-groups PEB model, a greedy search was implemented to prune away connections not contributing significantly to the free energy using BMR. Fig 4 shows the most parsimonious models and Fig 5 shows the estimated log scaling parameters contrasting healthy controls with UWS PET- (A), MCS+ with UWS PET- (B), and finally, healthy controls with MCS+ (C). Here, we applied a threshold of >.99 for the posterior probability; in other words, connections that were pruned by BMR and connections with lower than .99 posterior probability with their respective log scaling parameter are faded out (Fig 5A–5C).

On inverting the DMN for the control and UWS PET- groups, 3 connections were pruned away by BMR with additional 4 connections having lower than .99 posterior probability (Figs 4A and 5A). All but one of the pruned connections were located within the posterior cortices between lateral parietal cortices and PCC/precuneus (except for the right backward frontoparietal connection). The largest reduction in effective connectivity was located on left frontoparietal connection; the backward connection between mPFC and left lateral parietal node was largely diminished for the UWS PET- group in comparison to healthy controls.

On inverting the DMN contrasting MCS+ and UWS PET-, only three connections survived the BMR process with at least .99 posterior probability (with additional three connections surviving pruning with lower than .99 posterior probability; Figs 4B and 5B). As with the control vs. UWS PET- contrast, the largest reduction was on the left backward connectivity from mPFC to lLP, with left lLP-mPFC forward connectivity increasing.

On inverting the DMN for the contrast between healthy controls and MCS+, two connections were pruned by the BMR with additional 4 connections having lower than .99 posterior probability for being present (Figs 4C and 5C). The largest reductions were between the posterior nodes, to and from the lateral parietal cortices and PCC/precuneus. In addition, the left frontoparietal backward connectivity was reduced, although with smaller than .99 posterior probability and with clearly smaller effect size than with UWS PET-. Other non-pruned connections were associated with small to medium increases.

In addition, we also observed increased connectivity (relatively small effect sizes) in most of the other connections with at least .99 posterior probability.

Leave-one-subject-out cross-validation

To conduct LOSOCV, the DCM model was inverted again, this time separately for each patient group. Following the inversion process, PEB was conducted repeatedly on the training set in each cross-validation run alongside LOSOCV analysis to generate the posterior probabilities for group-membership (see Methods).

First, the UWS PET- patients were classified alongside the controls based on the full DMN model, and two hypothesis-driven connection subsets (frontoparietal- and parietal connections; Fig 6). A similar approach was applied classifying MCS+ patients alongside UWS PET- patients, and finally, healthy controls alongside MCS+ patients. Figs 6 and 7 show violin plots representing the individual posterior probabilities for the hypothesis-driven classifications and data-driven approach, for all three contrasts, respectively (A: control vs. UWS PET-, B: MCS + vs. UWS PET-, C: control vs. MCS+). As seen in Fig 6, frontoparietal connections classified correctly most of the controls and MCS+, and around half of the UWS PET- patients in the
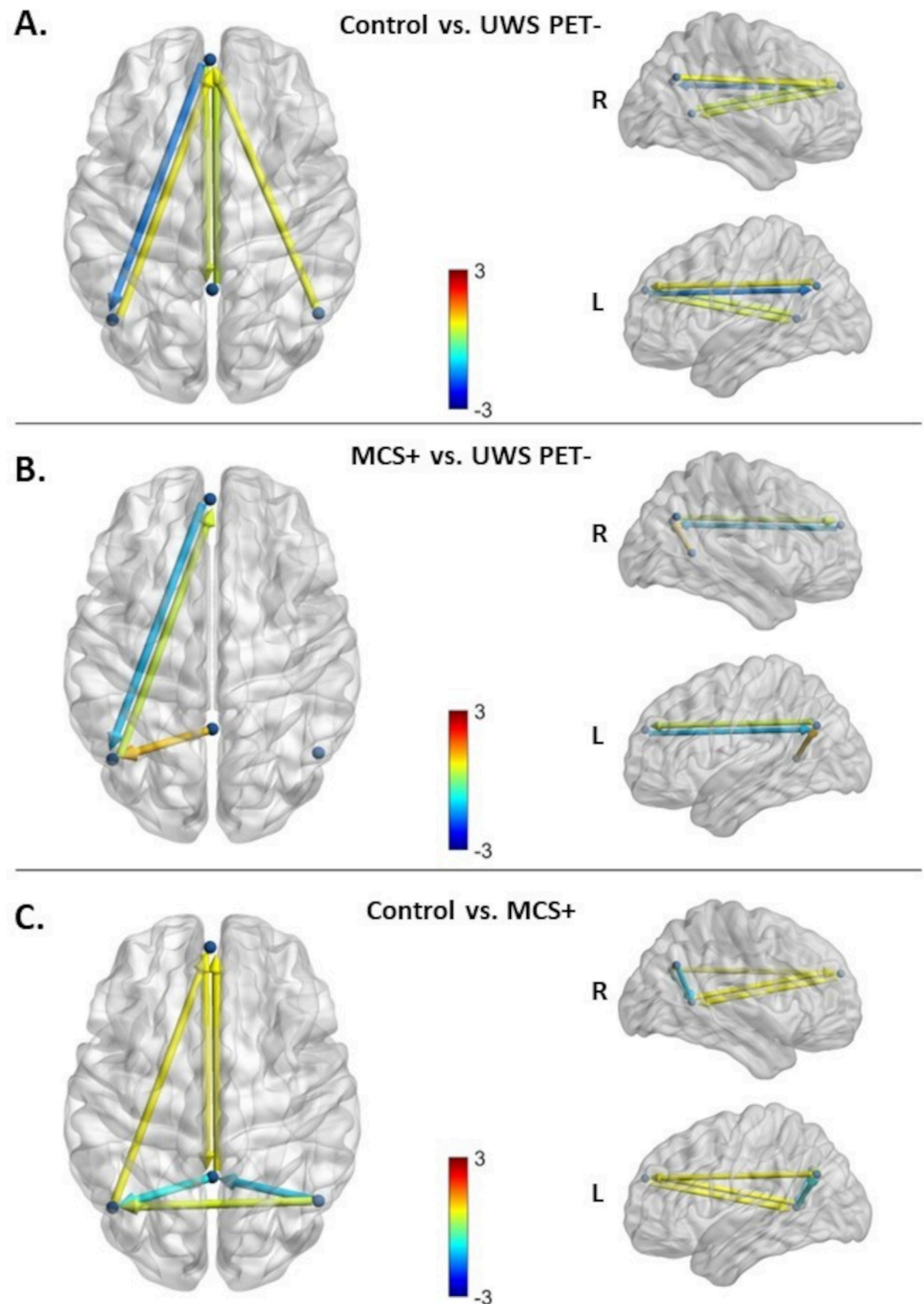
Fig 4. The most parsimonious DMN models after BMA and BMR contrasting the healthy controls (HC) and the UWS PET-, MCS+ patients and UWS PET-, and healthy controls and MCS+. Color shows modulation strength and direction. All panels express the modulations of couplings for the latter state relative to the first. **A.** The most parsimonious model best explaining the difference between healthy controls and UWS PET- patients. Three connections were pruned with an additional four having lower than .99 posterior probability of being present. All but one pruned connection was located between lateral parietal and PCC/precuneus nodes. When moving from the state of healthy controls to UWS PET-, the largest reduction in effective connectivity was in the backward connection from the medial prefrontal cortex to left lateral parietal cortex. **B.** The most parsimonious model best explaining the difference between the MCS+ and UWS PET-

patients. Six connections were pruned by the BMR with an additional three connections having lower than .99 posterior probability of being present. When moving from UWS PET- to MCS+, the largest reduction was observed on the backward connection from the medial prefrontal cortex to left lateral parietal cortex, similar to the reduction between healthy controls and UWS PET- patients. **C.** The most parsimonious model explaining the difference between healthy controls and MCS+ patients. Two connections were pruned with additional four connections having lower than .99 posterior probability of being present. When moving from the state of healthy controls to MCS+, the largest reductions on effective connectivity were on posterior connections between the lateral parietal cortices and PCC/precuneus.

controls vs. UWS PET- and MCS+ vs. UWS PET- contrasts. Both full DMN and parietal subsets clustered most of the subjects around the chance level of 0.5. We further produced confusion matrices of prediction accuracy calculated by labelling posterior probabilities greater than 0.5 as a positive classification (for both hypothesis-driven subsets and the data-driven approach). See S3, S4 Figs in S1 Text.
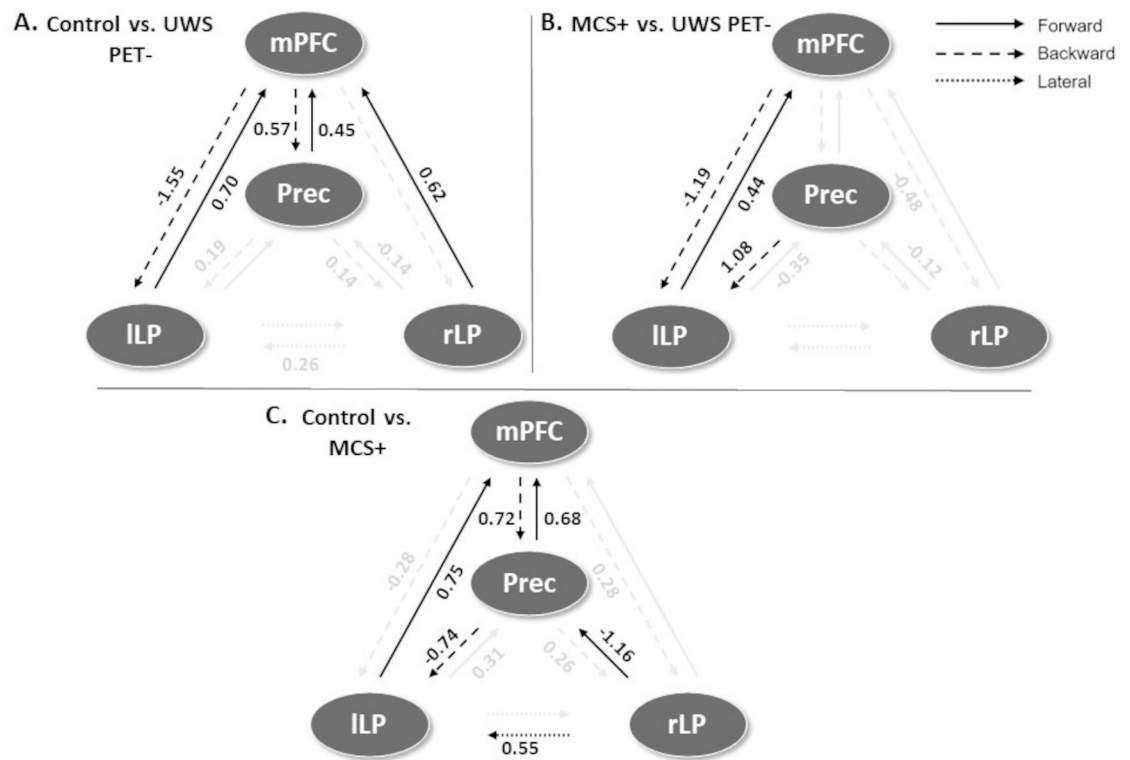
Fig 5. The corresponding log scaling parameters for the connection strengths in the DMN after BMR and BMA. Positive values represent an increase and negative values a decrease in effective connectivity for the three group comparisons. Connections that were pruned by BMR and connections with lower than .99 posterior probability with their respective log scaling parameter are faded out. **A.** The modulatory effects best explaining the difference between healthy controls (HC) and UWS PET- patients. Connectivity between lateral parietal and PCC/precuneus nodes were either pruned away by BMR or had lower than .99 posterior probability with low modulatory effects. The largest reduction was found on backward lateral frontoparietal connection from medial prefrontal cortex to left lateral parietal cortex. **B.** The modulatory effects best explaining the difference between MCS+ and UWS PET-. The modulatory effects on left bidirectional frontoparietal connections were both in the same direction as when comparing healthy controls to UWS PET-, with the largest reduction on left backward frontoparietal connection. In addition, right backward frontoparietal connectivity and posterior forward connectivity between lateral parietal nodes and PCC/precuneus reduced (smaller effect sizes), albeit with lower than .99 posterior probability of being present. **C.** The modulatory effects best explaining the difference between healthy controls and MCS+. The largest reductions were between the posterior nodes, between the lateral parietal nodes and PCC/precuneus. Bidirectional medial frontoparietal connectivity was increased in MCS+ in comparison to healthy controls. mPFC–medial prefrontal cortex, Prec–posterior cingulate cortex/precuneus, lLP–left lateral parietal cortex, rLP–right lateral parietal cortex.
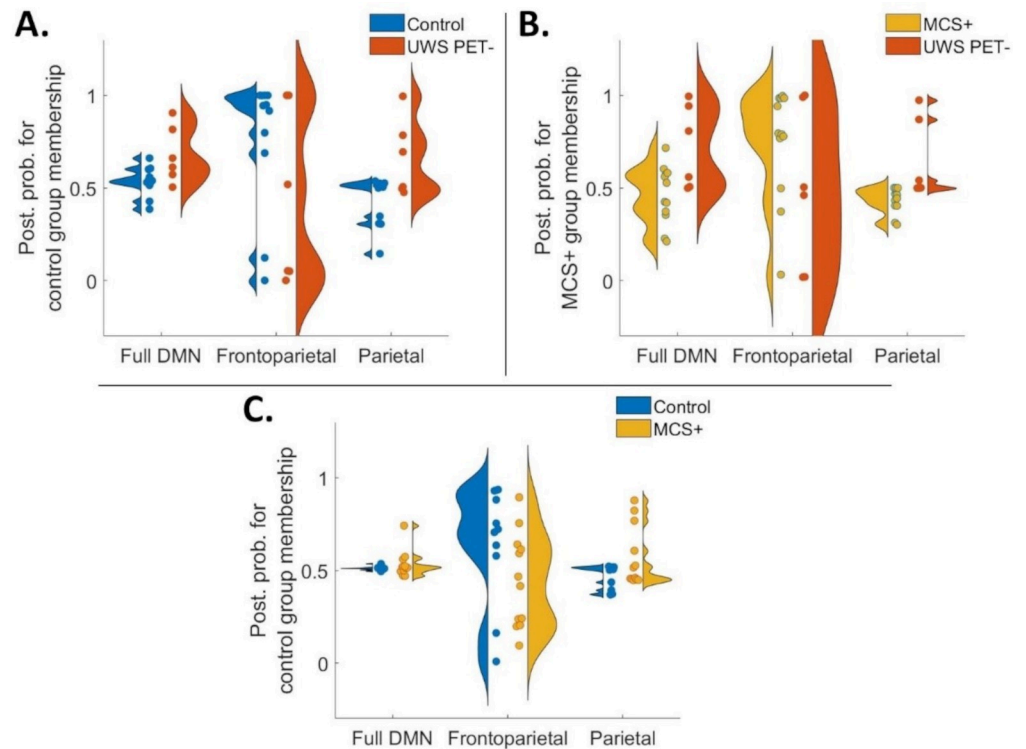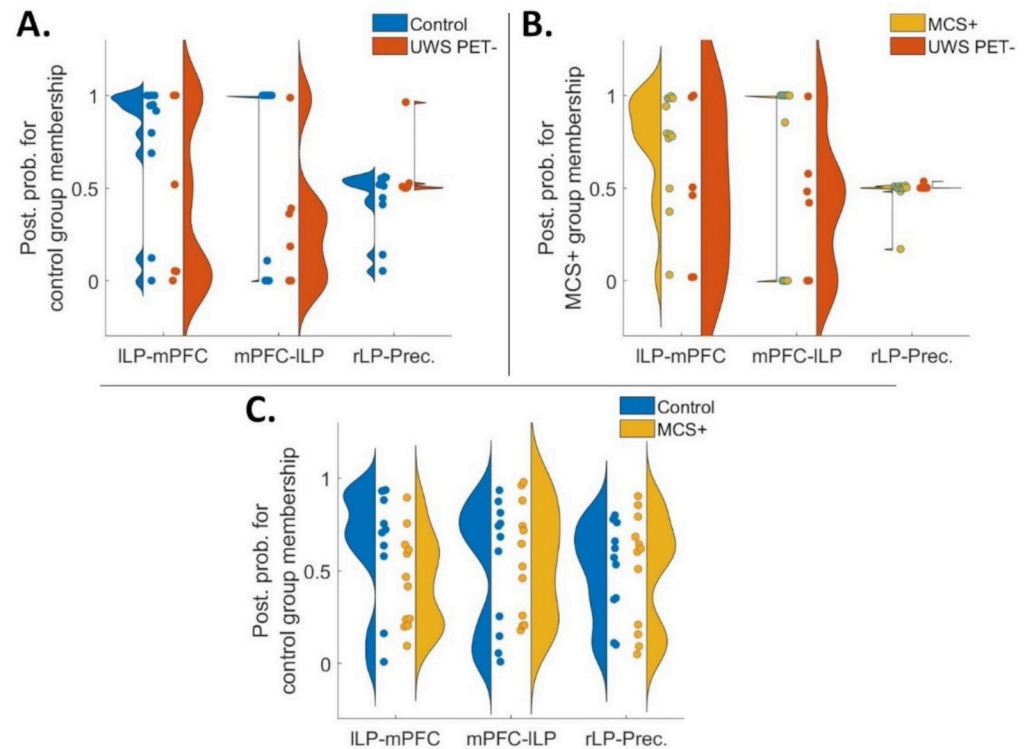
Fig 6. Violin plots representing diversity in posterior probabilities for healthy control group membership (A and C) and for MCS+ group membership (B) for the hypothesis-driven subsets for all three group contrasts. Each colored point specifies a subject. In a perfect model in panels A and B, the UWS PET- patients ($N = 6$), and in panel C, the MCS+ patients ($N = 12$) should approach a posterior probability of zero. Overall, the results show a trend for frontoparietal connections producing the best predictions. **A.** When classifying UWS PET- patients alongside healthy controls, the frontoparietal subset produced the best results. The individual data points reveal more consistent classifications of healthy controls. On all three panels, full DMN model and parietal subset produced classifications with most posterior probabilities bordering the 0.5 chance level. **B.** As in panel A, the best predictions when classifying UWS PET- patients alongside MCS+ were based on frontoparietal connections, specifically with MCS+ patients. **C.** Classification of MCS+ alongside healthy controls. Frontoparietal subset produced the best predictions, however with large variability on the performance across the subjects.

https://doi.org/10.1371/journal.pone.0298110.g006

We then moved to a data-driven approach in which we first predicted the patient group membership based on the connections with the largest reductions in PEB, one at a time, working through all connections. Lastly, we checked combinations based on the connections' respective classification accuracies (see Methods). The bi-directional left frontoparietal connectivity produced the best predictions, especially when classifying the UWS PET- from both, healthy controls and the MCS+ patients (Fig 7A and 7B), with the best predictions based on the backward mPFC-lLP connectivity. Forward lLP-mPFC connectivity produced the best predictions for controls vs. MCS+ contrast, especially for the healthy controls (7C). None of the tested combinations improved classification performance.

Leave-one-state-out cross-validation

Finally, the predictive power of DCM modelling was generalized in two more difficult classification problems; each model was trained first on healthy controls and UWS PET- and then tested on the previously unseen UWS PET + group. A similar approach was used with a training set consisting of MCS+ and UWS PET- patients. The individual posterior probabilities for the five UWS PET + patients represented in a violin plot for both, the hypothesis subsets
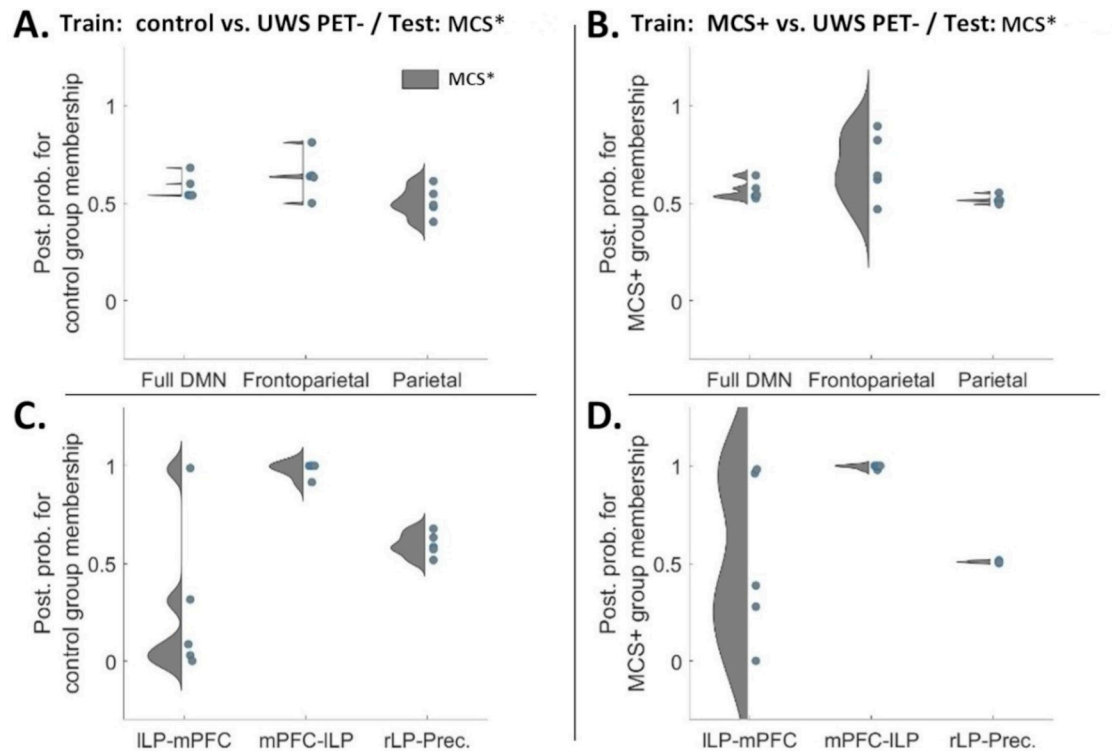
Fig 7. Violin plots representing diversity in posterior probabilities for control group membership (A and C) and for MCS+ group membership (B) for the data-driven connections for all three contrasts. Each colored point specifies a subject. In a perfect model in panels A and B, the UWS PET- patients, and in panel C, the MCS+ patients should approach a posterior probability of zero. Overall, the best predictive performance was based on the left bi-directional frontoparietal connections when classifying UWS PET- alongside controls (A) and MCS+ (B). Largest inconsistencies and variability were on classifications of MCS+ alongside healthy controls. **A.** Left frontoparietal connectivity from mPFC to lLP produced the best predictions (mean posterior probabilities) of the group-membership when classifying UWS PET- alongside healthy controls. As with the hypothesis-driven subsets, the classifications were more accurate with healthy controls than with patients. **B.** As in panel A with healthy controls and UWS PET- patients, the classification performances based on mPFC-lLP and lLP-mPFC produced the most consistent results when contrasting UWS PET- patients alongside MCS+. **C.** Mean posterior probabilities for classification of MCS+ alongside healthy controls. The performance of the models based on the single connections did not produce consistently accurate classifications. mPFC–medial prefrontal cortex, Prec–posterior cingulate cortex/precuneus, lLP–left lateral parietal cortex, rLP–right lateral parietal cortex.

https://doi.org/10.1371/journal.pone.0298110.g007

(panels A and B; controls vs. UWS PET- and controls vs. MCS+, respectively) and for data-driven connections (panels C and D) are shown in Fig 8. The hypothesis-driven subsets did not classify the MCS* as controls or MCS+. Instead, when trained on datasets from healthy controls and UWS PET-, the frontoparietal subset classified four out of five MCS* patients as UWS PET-.

With the data-driven approach, the left backward frontoparietal connectivity from mPFC to lLP produced nearly perfect predictions classifying the MCS* datasets as controls (8C, p (control|MCS* > .92) and MCS+ (8D, p(MCS+|MCS* > .98) rather than as UWS PET- group. Similar as with frontoparietal subset (8A), the left forward connectivity from lLP to mPFC classified four of five patients as UWS PET- patients rather than healthy controls –three of them with a high posterior probability. This dissociation was not as prominent when training the model with MCS+ and UWS PET- patients (8D); the backward connectivity still produced nearly perfect classifications (of MCS* as MSC+) while the predictions based on the forward connectivity showed larger variability.

Fig 8. Violin plots representing diversity in posterior probabilities for control group membership (A and C) and for MCS+ group membership (B and D) for both, the hypothesis- and data-driven predictions. Here, the models were trained on datasets from controls and UWS PET- (A & C) or from MCS+ and UWS PET- (B and D) and tested on unseen data from MCS* patients ($N = 5$). Each colored point specifies a subject. Overall, the left backward frontoparietal connectivity produced the best group membership predictions. **A and B.** Mean posterior probabilities for classification of MCS* patients alongside healthy controls (A) and MCS + patients (B). Neither of the hypothesis-driven subsets, nor the full DMN, clearly classified the unseen MCS* patients as members of either train-group. **C and D.** Left frontoparietal connectivity from mPFC to lLP produced almost perfect predictions for the MCS*, classifying all five patients as either controls or MCS+ rather than UWS PET- patients. Unlike the backward connectivity, predictions based on the left forward connectivity from lLP to mPFC, the model classified four of five MCS* patients as UWS PET- rather than as controls (C). Similarly, when trained on MCS+ and UWS PET-, the model classified three of five patients as UWS PET- rather than MCS+. mPFC–medial prefrontal cortex, Prec–posterior cingulate cortex/precuneus, lLP–left lateral parietal cortex, rLP–right lateral parietal cortex.

https://doi.org/10.1371/journal.pone.0298110.g008

Discussion

In this cross-sectional, retrospective analysis, we applied spectral DCM to high-density EEG data with PEB to investigate the difference in effective connectivity dynamics between cortico-cortical regions of the DMN in DoC patients (UWS, MCS+, and MCS*) and healthy controls. Overall, the modelling results indicate a key difference between healthy controls or MCS + patients and unresponsive patients with compatible hypometabolism (UWS PET-) in left-hemispheric backward frontoparietal connectivity. Furthermore, with out-of-sample cross-validation, we demonstrated that this association is robust enough to not only distinguish patient groups from each other, but also generalizes to an unseen data subset, collected from seemingly unresponsive patients showing preserved brain activity compatible with MCS (MCS*). These results identify specific alterations in the DMN after severe brain injury and highlight the clinical utility of EEG-based measurement of effective connectivity for identifying covert consciousness.

Dynamic causal modelling

The most parsimonious model explaining the difference between healthy controls and unresponsive patients with congruent hypometabolism (UWS PET-) indicated a large relative reduction in left-hemisphere backward frontoparietal connectivity in UWS PET- patients. Additionally, a small, lower-probability reduction from right lateral parietal cortex to precuneus was found. Interestingly, excluding the right parietal connection, the estimated connectivity in the posterior nodes–within the 'posterior hot zone of conscious contents' [63, 64]–was either pruned away from the model best explaining the difference or returned only small, low-probability increases suggesting lower relative importance for the posterior hot zone in explaining the difference between healthy controls and UWS PET- patients. Generally, connections pruned by BMR are considered not to contribute towards the model evidence [65]. In contrast, in a previous fMRI DCM study with DoC patients, precuneus/PCC-related connectivity reduction was the key difference; specifically, the recurrent connectivity (down-regulation of the PCC itself) was found to be diminished on UWS patients in comparison to both, MCS patients and healthy controls [25].

However, not only are the data between Crone colleagues' study [25] and the present study from different modalities, and thus, direct comparisons of the results unsound, the underlying neurobiologically motivated models used by DCM are different for hemodynamic vs. electrophysiological data leading to a different interpretation of the modulatory effects. The interpretation of the modulatory effects in DCM for fMRI vs. EEG differ in that positive and negative values indicate excitatory and inhibitory effects in fMRI data (except for recurrent connections, for which the connection strength is always negative and modulations reflect increases or decreases in comparison to the prior). In DCM for EEG, positive modulations indicate an increase and negative a decrease in connectivity relative to the prior. In the neural mass model we used here, the backward connections are thought to have more inhibitory and largely modulatory effect in the nodes they target (top-down connections), while forward connections are viewed as having a strong driving effect (bottom-up) [46, 47].

Here, we modelled the data using the default DCM settings for ERP neuronal model [55]) primarily in order to produce comparable results with prior DCM for EEG work modelling consciousness [28, 66, 67]. Further, we aimed to model disrupted consciousness at the level of active networks rather than focusing on e.g., synaptic hypotheses or recurrent self-connections (intrinsic connectivity), which could be better captured with other neuronal models such as the local field potential model [68] or the Canonical Microcircuits model [69], see also [45] for a review of neuronal population models). Hence, we only estimated extrinsic connectivity–i.e., connectivity between cortical areas. It is possible that the observed differences in the network dynamics are driven by modulations in self-inhibiting, recurrent connectivity within the cortical sources or within and between subcortical networks driving the disruptions in the DMN [26, 27]. A worthwhile endeavor for future DCM for EEG studies would be to model the extent to which recurrent, within-source cortical connectivity may or may not drive the modulations in extrinsic connectivity.

To the best of our knowledge, only one study has used DCM for EEG in DoC populations. Boly and colleagues [28] showed that in an auditory mismatch negativity paradigm, the difference between UWS, MCS, and healthy controls was an impairment of backward connectivity from frontal to temporal cortices in the UWS patients, emphasizing the importance of top-down processing for conscious perception. Similarly, in the present resting-paradigm, the key difference distinguishing UWS PET- from both, MCS+ and healthy controls was decreased left-lateralized backward frontoparietal connectivity in UWS PET- patients, although from medial prefrontal cortex to lateral parietal cortex and not to superior parietal cortex. It is

important to note, however, that the differences in the paradigm, methodology and in the models estimated render rigorous, direct comparisons of the results between [28] and the present study infeasible. Moreover, even though some of the patients may have been the same between the present study and those in [28], the data were different (here recorded with high-density EEG during PET while Boly and colleagues used a 64 channel EEG prior to TMS-EEG). Despite the methodological differences, the results of both studies suggest a crucial role for lateral backward connectivity originating from the frontal cortex. Future studies should investigate this further by modelling the connectivity related to temporal areas, and the backward frontoposterior connectivity in other resting networks (see below) in DoC patients.

Like with healthy controls vs. UWS PET- comparison, the largest difference between MCS + and UWS PET- patients was left frontoparietal backward connectivity, with UWS PET-patients again showing reduced connectivity. Furthermore, the left forward parietofrontal connectivity and backward connectivity from precuneus to lLP both increased, reproducing the modulations between healthy controls and UWS PET-. These changes were accompanied by smaller, low-probability reductions in forward connectivity within the posterior hot zone and in right backward frontoparietal connectivity. These modelling results highlight the left fronto-parietal backward connectivity as the key distinguishing difference when comparing healthy controls or conscious patients with unconscious patients and complement those of previous studies discriminating DoC patients from scalp-level EEG connectivity; especially frontal and parietal functional connectivity has been shown to consistently discriminate DoC patients [9, 31]. As the direction and the spatial location of the changes in connectivity were similar with the comparisons involving UWS PET- patients, and distinguishable from those when comparing healthy controls vs. MCS+, we were motivated to further test the predictive power of the modulatory effects (see below).

In contrast, the largest connectivity reductions between healthy controls and MCS+, although relatively smaller than in previous contrasts, were associated with the precuneus node in the posterior hot zone. The left backward frontoparietal connectivity was again reduced, but by a smaller effect and with lower than .99 probability of being present in the most parsimonious model. The activity changes in the posterior hot zone of conscious content have been associated with changes in consciousness not only during sleep [64, 70] and general anesthesia [67, 71], but also in DoC patients [17, 72]. Moreover, previous studies have suggested a subdivision of the frontoparietal network into two anticorrelated subnetworks; an "intrinsic" network encompassing precuneus/PCC, anterior cingulate/mesofrontal cortices, and parahippocampal areas associated with internal awareness, and into an "extrinsic" central executive network encompassing dorsolateral prefrontal and posterior parietal areas linked with the intensity of external awareness [73, 74]. The observed decrease in the left lateral frontoparietal connectivity in the present study between UWS PET- patients and healthy controls or MCS+ patients may reflect such diminished internal awareness in the UWS PET- patients. To that end, future endeavors should investigate the modulatory effects and the possible predictive power of such modulations in other resting state networks, such as the central executive network.

However, changes in the physiological state of the frontoparietal network alter not only consciousness but also several other brain functions such as vigilance and attention [63, 75]. Moreover, the specific areas of the DMN have been associated with specific cognitive functions; for example, the frontal areas seem to be important for self-reference, whereas the precuneus/PCC in autobiographical memory [76]. It remains a possibility that the found modulations in the DMN reflect changes also in other cognitive functions, rather than in awareness alone.

It is important to bear in mind that DoC patients typically suffer from widespread structural brain damage often accompanied by distributed white matter anomalies [12, 14, 77]. Hence, it

is relevant to consider the feasibility and validity of applying DCM to DoC patients; this is particularly true for DCM for EEG which requires the specification of the anatomical locations of the nodes/sources a priori, and with patients with non-traumatic etiology, e.g., patients with anoxic brain damage [78, 79]. Here, we mitigated these concerns first by limiting our modelling to DMN, a resting state network previously associated with DoC [8, 13, 14, 17, 25, 49, 50, 80, 81] and with changes in the conscious state e.g., due to anesthesia [73, 82, 83] and sleep [84].

Second, we selected only patients with TBI as compared to non-traumatic etiologies, it has been associated with more focal injury centered often on areas susceptible to rotational forces, such as the brainstem, midbrain, thalamus, hypothalamus, cerebellum, and posterior corpus callosum [15, 85]. That said, future studies should look to extend these results to other etiologies; an obvious downside for trying to control for the individual differences due to brain damage by restricting the analysis to TBI patients only, was reduced sample size. By including other etiologies, future studies could not only aim to replicate and verify these results with larger samples and better power, but to increase the potential clinical utility by extending them to cover larger patient populations.

Third, we applied a special case of Bayesian model selection (BMS), Bayesian model reduction (BMR), to invert multiple nested models from a single, fully connected DMN (see Methods). A particular advantage here is that BMR can be applied using an explanatory approach, in which no strong a priori hypotheses about the model parameters are needed. This enables a greedy search to compare the negative free energies of the reduced (nested) models by iteratively discarding parameters that do not contribute to the free energy. The procedure stops when discarding any parameters starts to decrease the negative free energy, returning the model that most effectively trades-off goodness of fit and model complexity in explaining the data. BMR applied in this way allows one to estimate a large model space from a single, specified full model in a relatively short period of time [59, 60, 65].

Nevertheless, it is possible that not all true influences on the specific regions are captured by the specified full model. Moreover, the explanatory approach to BMR is conducted under the assumption that all reduced models are equally probable a priori, and thus, the full model should only contain parameters that are biologically plausible. Here, we cannot exclude physical damage to cortical areas and pathways crucial to the functioning of the DMN. In addition, the spatial accuracy of our model was further limited by the use of template MRI mesh–future studies should include rigorously examined data about the extent and location of the structural damage in the patient cohort in addition to electronically digitizing the individual head-surface points to improve the spatial accuracy of the models.

That said, our aim was not to make any strong claims about the "true" model; to draw stronger conclusions about the "true" underlying neuronal basis using DCM for EEG, structural MRI imaging assessing the extent of the damage in specific patients, possibly in adjunct with source localization of the EEG signals with accurate co-registration between the EEG and the individual MRI data, should be applied. Here, the aim was to demonstrate and to compare the predictive performance of effective connectivity in the clinical context. Additionally, demonstrating predictive value with significant generalization performance with cross-validation, the level of confidence we can ascribe to our modelling results increases.

Leave-one-subject/state-out cross-validation (LOSOCV)

To test whether the effective connectivity modulations were consistent enough across the patient groups and healthy controls to reliably distinguish the groups from each other, we first conducted a leave-one-subject-out cross-validation based on hypothesis- (full DMN,

frontoparietal, and parietal subsets; Fig 6) and data-driven subsets of connections (Fig 7). Amongst the connection subsets, the frontoparietal connections performed the best, classifying most controls and MCS+, and half of the MCS* patients correctly in the healthy controls vs. UWS PET- and in MCS+ vs. UWS PET- contrasts. The full DMN and parietal subsets clustered most of the subjects around the chance level in all three contrasts.

We then moved to a data-driven approach in which we first predicted the patient group membership based on the connection with the largest reduction in PEB, one at a time, working through all connections. It is important to note that searching for the best connection in this way increases the risk of overfitting the model by potentially extracting some of the residual variation–noise–as if representing the underlying model structure. However, the fact that the best model generalized to an unseen dataset suggests that the results may reflect a genuine effect (see below).

With the data-driven approach, the bi-directional left frontoparietal connectivity produced the best predictions, especially when classifying the UWS PET- from both, healthy controls and the MCS+ patients. The single best performing connection was the backward frontoparietal connectivity (Fig 7). Not surprisingly, the classifications were more accurate and consistent with healthy controls than with patients; classifications of patients suffering from severe brain damage, and thus, from highly disrupted brain functioning, were expected to vary more than those of healthy controls. Next, we combined the single connections into data-driven subsets based on the classification performance: none of the combinations improved the performance of the single connections.

Last, the predictive power of DCM modelling was generalized in two more difficult classification problems; following the hypothesis- and data-driven approaches above, we trained each model on healthy controls or MCS+ on the one hand, and UWS PET- patients on the other, and then tested the models on the previously unseen, "covertly aware" MCS* patients. The hypothesis-driven subsets did not classify the MCS* patients as controls or MCS+. Crucially, with the data-driven approach, the left backward frontoparietal connection produced nearly perfect predictions classifying all five patients as either controls or MCS+ rather than UWS PET- patients. These results are compatible with previous PET imaging results by Thibaut and colleagues [4] who observed higher brain metabolism in the lateral and medial frontoparietal network in MCS* patients when compared to UWS PET- patients. Interestingly, their resting state EEG results with functional connectivity indicated a difference in the left hemisphere (and at the whole brain level) when comparing MCS* to both UWS PET- and to MCS patients. To that end, alpha connectivity was higher and delta connectivity lower in MCS* when compared to UWS PET- patients. Moreover, a difference between MCS* and MCS was observed in the left hemisphere with the latter having higher connectivity in the theta band. This finding further extended to MCS* vs. MCS+ comparison.

While the results of the present study should be interpreted with caution due to the relatively low number of subjects in our study, the results, in conjunction with those of Thibaut and colleagues [4] suggest a pivotal role for left hemisphere connectivity in distinguishing MCS* from UWS PET- and MCS patients. Furthermore, the present results highlight the importance of the frontoparietal connectivity–particularly the left-lateralized backward connectivity–when predicting these states of consciousness. The importance of frontoparietal connections within the DMN for dissociating states of consciousness in DoC patients is not surprising given the previously established association between conscious awareness and the DMN [13, 17, 73, 80]. More specifically, consciousness is thought to require brain-wide broadcasting of information by a "global workspace" associated with brain areas within the frontoparietal network [86–88].

It is important to note, however, that the global neuronal workspace theory (GNW) is not a localisationist approach but rather posits a distributed "router" for conscious access [88]. The extensive and rapid bidirectional connectivity between the hubs of the GNW is thought to trigger the sudden collective and coordinated activity mediating global broadcasting [89]. In brief, local cortical processors are linked by a core set of highly interconnected areas or hubs, which can select information from local processors, amplify it, and broadcast the information in a top-down matter to all other processors in the global workspace, rendering it conscious (and reportable). Aptly, these hubs initially included the prefrontal cortex and parietal cortex (in combination with a set of specialized and modular perceptual, motor, memory, evaluative, and attentional processors) although it has later been complemented with other, potentially equally important hubs (such as the anterior and posterior cingulate and the precuneus). If the feedforward signal generated by the local processers is strong enough, it reaches prefrontal cortex, which in turn triggers the ignition into the reverberant network, involving posterior parietal cortex in addition to other cortical and subcortical areas, such as the thalamus and cerebellum [89]. Without this global reverberant broadcasting–reflected on the backward feedback connectivity, the perceptual content will not enter conscious awareness. The novel finding here is the reduction in the long-range frontoparietal feedback connectivity that best predicts the state of consciousness when comparing unconscious patients to healthy controls or conscious patients. This observation is in accordance with the suggested importance of the connectivity between the hubs in the GNW.

However, it is important to keep in mind that presumably, when the patient becomes "more" conscious, different content becomes more globally available for conscious processing throughout the brain, affecting and employing different cognitive systems [75]. In other words, any major changes in the physiological state alter not only consciousness but other cognitive systems as well, many of which depend on levels of arousal-promoting neuromodulators. Therefore, it remains possible that the predictive performance of the frontoparietal effective connectivity is related not only to the state of consciousness, but also to other arousal-related cognitive processes. Further, it is worth noting that here, we limited our contrasts to MCS+, excluding minimally conscious- (minus) from the analyses. Our rationale was to include a second, irrefutably conscious control group. Nonetheless, future studies should include MCS- patients to better control for possible confounds of behavior and language functions present in MCS+. Indeed, modelling work such as in the present study can only estimate *what is included* in the model, and hence, it is possible that the modulations observed were driven by another brain source not included in the present estimated model. To highlight the importance of this point, previous studies have suggested partial spatial and functional reconfiguration of the DMN (and other resting networks) in addition to e.g. limbic hyperconnectivity in brain injured unresponsive patients [90, 91].

Moreover, conscious processing has been linked not only with alterations with the DMN, but in other resting networks too [50, 92]. It therefore remains possible that although we only modelled DMN connectivity–a resting network anticorrelated with e.g. left-lateralized frontotemporal "core" language network [93–95]–the modulations may have been driven by activity in other networks or in brain areas not included in our model. Future studies should not only expand on the resting networks investigated, but also thoroughly investigate the potential role the presence/lack of language ability may play on the connectivity modulations.

In summary, our results indicate a key difference between healthy controls or MCS + patients and unresponsive patients with congruent hypometabolism in left-lateralized backward frontoparietal connectivity. With out-of-sample cross-validation, we demonstrated that this association is robust enough to not only distinguish patient groups from each other, but also generalizes to an unseen data subset, collected from seemingly unresponsive patients.

These results contribute towards identifying specific alterations in network interaction after severe brain injury, and importantly, suggest clinical utility of EEG-based effective connectivity in identifying covertly aware patients who seem behaviorally unresponsive.

Supporting information

S1 Text. Data acquisition.
(DOCX)

Acknowledgments

Author Contributions

Conceptualization: Riku Ihalainen, Srivas Chennu.

Data curation: Jitka Annen, Olivia Gosseries, Rajanikant Panda, Aurore Thibaut, Steven Laureys.

Formal analysis: Riku Ihalainen.

Funding acquisition: Olivia Gosseries, Steven Laureys, Srivas Chennu.

Investigation: Riku Ihalainen, Jitka Annen, Olivia Gosseries, Charlotte Martial, Aurore Thibaut, Steven Laureys.

Methodology: Riku Ihalainen, Srivas Chennu.

Project administration: Olivia Gosseries, Steven Laureys, Srivas Chennu.

Resources: Steven Laureys, Srivas Chennu.

Software: Riku Ihalainen.

Supervision: Olivia Gosseries, Steven Laureys, Srivas Chennu.

Visualization: Riku Ihalainen.

Writing – original draft: Riku Ihalainen.

Writing – review & editing: Riku Ihalainen, Jitka Annen, Olivia Gosseries, Paolo Cardone, Rajanikant Panda, Charlotte Martial, Aurore Thibaut, Steven Laureys, Srivas Chennu.

References

1. Laureys S. et al., "Unresponsive wakefulness syndrome: A new name for the vegetative state or apallic syndrome," *BMC Medicine*, vol. 8, pp. 2–5, 2010, https://doi.org/10.1186/1741-7015-8-68 PMID: 21040571

2. Bruno M. A., Vanhaudenhuyse A., Thibaut A., Moonen G., and Laureys S., "From unresponsive wakefulness to minimally conscious PLUS and functional locked-in syndromes: Recent advances in our understanding of disorders of consciousness," *Journal of Neurology*, vol. 258, no. 7, pp. 1373–1384, 2011, https://doi.org/10.1007/s00415-011-6114-x PMID: 21674197

3. Stender J. et al., "Diagnostic precision of PET imaging and functional MRI in disorders of consciousness: A clinical validation study," *The Lancet*, vol. 384, no. 9942, pp. 514–522, 2014, https://doi.org/10.1016/S0140-6736(14)60042-8 PMID: 24746174

4. Thibaut A. et al., "Preservation of Brain Activity in Unresponsive Patients Identifies MCS Star," *Annals of Neurology*, vol. 90, no. 1, pp. 89–100, 2021, https://doi.org/10.1002/ana.26095 PMID: 33938027

5. van Erp W. S., Lavrijsen J. C. M., Vos P. E., Bor H., Laureys S., and Koopmans R. T. C. M., "The vegetative state: Prevalence, misdiagnosis, and treatment limitations," *Journal of the American Medical Directors Association*, vol. 16, no. 1, p. 85.e9–85.e14, 2015, https://doi.org/10.1016/j.jamda.2014.10.014 PMID: 25528282

6. Demertzi A. et al., "Intrinsic functional connectivity differentiates minimally conscious from unresponsive patients," *Brain*, vol. 138, no. 9, pp. 2619–2631, 2015, https://doi.org/10.1093/brain/awv169 PMID: 26117367

7. Di Perri C. et al., "Neural correlates of consciousness in patients who have emerged from a minimally conscious state: A cross-sectional multimodal imaging study," *The Lancet Neurology*, vol. 15, no. 8, pp. 830–842, 2016, https://doi.org/10.1016/S1474-4422(16)00111-3 PMID: 27131917

8. Laureys S. et al., "Impaired effective cortical connectivity in vegetative state: Preliminary investigation using PET," *NeuroImage*, vol. 9, no. 4, pp. 377–382, 1999, https://doi.org/10.1006/nimg.1998.0414 PMID: 10191166

9. Chennu S. et al., "Spectral Signatures of Reorganised Brain Networks in Disorders of Consciousness," *PLoS Computational Biology*, vol. 10, no. 10, 2014, https://doi.org/10.1371/journal.pcbi.1003887 PMID: 25329398

10. King J. R. et al., "Information sharing in the brain indexes consciousness in noncommunicative patients," *Current Biology*, vol. 23, no. 19, pp. 1914–1919, 2013, https://doi.org/10.1016/j.cub.2013.07.075 PMID: 24076243

11. Sitt J. D. et al., "Large scale screening of neural signatures of consciousness in patients in a vegetative or minimally conscious state," *Brain*, vol. 137, no. 8, pp. 2258–2270, 2014, https://doi.org/10.1093/brain/awu141 PMID: 24919971

12. Annen J. et al., "Regional brain volumetry and brain function in severely brain-injured patients," *Annals of Neurology*, vol. 83, no. 4, pp. 842–853, 2018, https://doi.org/10.1002/ana.25214 PMID: 29572926

13. Boly M. et al., "Functional connectivity in the default network during resting state is preserved in a vegetative but not in a brain dead patient," *Human Brain Mapping*, vol. 30, no. 8, pp. 2393–2400, 2009, https://doi.org/10.1002/hbm.20672 PMID: 19350563

14. Fernández-Espejo D. et al., "A role for the default mode network in the bases of disorders of consciousness," *Annals of Neurology*, vol. 72, no. 3, pp. 335–343, 2012, https://doi.org/10.1002/ana.23635 PMID: 23034909

15. Guldenmund P. et al., "Structural brain injury in patients with disorders of consciousness: A voxel-based morphometry study," *Brain Injury*, vol. 30, no. 3, pp. 343–352, 2016, https://doi.org/10.3109/02699052.2015.1118765 PMID: 26890670

16. Soddu A. et al., "Identifying the default-mode component in spatial IC analyses of patients with disorders of consciousness," *Human Brain Mapping*, vol. 33, no. 4, pp. 778–796, 2012, https://doi.org/10.1002/hbm.21249 PMID: 21484953

17. Vanhaudenhuyse A. et al., "Default network connectivity reflects the level of consciousness in non-communicative brain-damaged patients," *Brain*, vol. 133, no. 1, pp. 161–171, 2010, https://doi.org/10.1093/brain/awp313 PMID: 20034928

18. Stender J. et al., "The Minimal Energetic Requirement of Sustained Awareness after Brain Injury," *Current Biology*, vol. 26, no. 11, pp. 1494–1499, 2016, https://doi.org/10.1016/j.cub.2016.04.024 PMID: 27238279

19. Stender J. et al., "Quantitative rates of brain glucose metabolism distinguish minimally conscious from vegetative state patients," *Journal of Cerebral Blood Flow and Metabolism*, vol. 35, no. 1, pp. 58–65, 2015, https://doi.org/10.1038/jcbfm.2014.169 PMID: 25294128

20. Thibaut A. et al., "Metabolic activity in external and internal awareness networks in severely brain-damaged patients," *Journal of Rehabilitation Medicine*, vol. 44, no. 6, pp. 487–494, 2012, https://doi.org/10.2340/16501977-0940 PMID: 22366927

21. Aubinet C. et al., "Brain Metabolism but Not Gray Matter Volume Underlies the Presence of Language Function in the Minimally Conscious State (MCS): MCS+ Versus MCS− Neuroimaging Differences," *Neurorehabilitation and Neural Repair*, vol. 34, no. 2, pp. 172–184, 2020, https://doi.org/10.1177/1545968319899914 PMID: 31971884

22. Bruno M. A. et al., "Functional neuroanatomy underlying the clinical subcategorization of minimally conscious state patients," *Journal of Neurology*, vol. 259, no. 6, pp. 1087–1098, 2012, https://doi.org/10.1007/s00415-011-6303-7 PMID: 22081100

23. Thibaut A., Bodien Y. G., Laureys S., and Giacino J. T., "Minimally conscious state 'plus': diagnostic criteria and relation to functional recovery," *Journal of Neurology*, vol. 267, no. 5, pp. 1245–1254, 2020, https://doi.org/10.1007/s00415-019-09628-y PMID: 31773246

24. Laureys S., Owen A. M., and Schiff N. D., "Brain function in brain death, coma, vegetative state, minimally conscious state and locked-in syndrome," *Lancet Neurology*, vol. 3, no. 9, pp. 537–546, 2004.

25. Crone J. S. et al., "Impaired consciousness is linked to changes in effective connectivity of the posterior cingulate cortex within the default mode network," *NeuroImage*, vol. 110, pp. 101–109, 2015, https://doi.org/10.1016/j.neuroimage.2015.01.037 PMID: 25620493

26. Chen P. et al., "Abnormal Effective Connectivity of the Anterior Forebrain Regions in Disorders of Consciousness," *Neuroscience Bulletin*, vol. 34, pp. 647–658, 2018, https://doi.org/10.1007/s12264-018-0250-6 PMID: 29959668

27. Coulborn S., Taylor C., Naci L., Owen A. M., and Fernández-Espejo D., "Disruptions in effective connectivity within and between default mode network and anterior forebrain mesocircuit in prolonged disorders of consciousness," *Brain Sciences*, vol. 11, no. 6, 2021, https://doi.org/10.3390/brainsci11060749 PMID: 34200092

28. Boly M. et al., "Preserved Feedforward But Impaired Top-Down Processes in the Vegetative State," *Science Reports*, vol. 332, pp. 858–862, 2011.

29. Bodart O. et al., "Measures of metabolism and complexity in the brain of patients with disorders of consciousness," *NeuroImage*: *Clinical*, vol. 14, pp. 354–362, 2017, https://doi.org/10.1016/j.nicl.2017.02.002 PMID: 28239544

30. Claassen J. et al., "Detection of Brain Activation in Unresponsive Patients with Acute Brain Injury," *New England Journal of Medicine*, vol. 380, no. 26, pp. 2497–2505, 2019, https://doi.org/10.1056/NEJMoa1812757 PMID: 31242361

31. Chennu S. et al., "Brain networks predict metabolism, diagnosis and prognosis at the bedside in disorders of consciousness," *Brain*, vol. 140, no. 8, pp. 2120–2132, 2017, https://doi.org/10.1093/brain/awx163 PMID: 28666351

32. Cruse D. et al., "Bedside detection of awareness in the vegetative state: A cohort study," *The Lancet*, vol. 378, no. 9809, pp. 2088–2094, 2011, https://doi.org/10.1016/S0140-6736(11)61224-5 PMID: 22078855

33. Lechinger J. et al., "Mirroring of a simple motor behavior in Disorders of Consciousness," *Clinical Neurophysiology*, vol. 124, no. 1, pp. 27–34, 2013, https://doi.org/10.1016/j.clinph.2012.05.016 PMID: 22721652

34. Monti M. M. et al., "Willful modulation of brain activity in disorders of consciousness," *New England Journal of Medicine*, vol. 362, no. 7, pp. 579–589, 2010, https://doi.org/10.1056/NEJMoa0905370 PMID: 20130250

35. Owen A. M., Coleman M. R., Boly M., Matthew H. D., Laureys S., and Pickard J. D., "Detecting awareness in the vegetative state," *Science*, vol. 313, no. 5792, pp. 1402–1402, 2006, https://doi.org/10.1126/science.1130197 PMID: 16959998

36. Owen A. M. and Coleman M. R., "Functional neuroimaging of the vegetative state," *Nature Reviews Neuroscience*, vol. 9, no. 3, pp. 235–243, 2008, https://doi.org/10.1038/nrn2330 PMID: 18285801

37. Schnakers C. et al., "Preserved covert cognition in noncommunicative patients with severe brain injury?," *Neurorehabilitation and Neural Repair*, vol. 29, no. 4, pp. 308–317, 2015, https://doi.org/10.1177/1545968314547767 PMID: 25160566

38. Gosseries O., Zasler N. D., and Laureys S., "Recent advances in disorders of consciousness: Focus on the diagnosis," *Brain Injury*, vol. 28, no. 9, pp. 1141–1150, Aug. 2014, https://doi.org/10.3109/02699052.2014.920522 PMID: 25099018

39. Carrière M. et al., "Auditory localization should be considered as a sign of minimally conscious state based on multimodal findings," *Brain Communications*, vol. 2, no. 2, p. fcaa195, Jul. 2020, https://doi.org/10.1093/braincomms/fcaa195 PMID: 33426527

40. Panda R. et al., "Posterior integration and thalamo-frontotemporal broadcasting are impaired in disorders of consciousness," *bioRxiv*, pp. 2021–11, 2021.

41. Kalmar K. and Giacino J. T., "The JFK Coma Recovery Scale—Revised," *Neuropsychological Rehabilitation*, vol. 15, no. 3–4, pp. 454–460, 2005, https://doi.org/10.1080/09602010443000425 PMID: 16350986

42. Nakayama N., Okumura A., Shinoda J., Nakashima T., and Iwama T., "Relationship between regional cerebral metabolism and consciousness disturbance in traumatic diffuse brain injury without large focal lesions: An FDG-PET study with statistical parametric mapping analysis," *Journal of Neurology*, *Neurosurgery and Psychiatry*, vol. 77, no. 7, pp. 856–862, 2006, https://doi.org/10.1136/jnnp.2005.080523 PMID: 16549415

43. Friston K. J., Bastos A., Litvak V., Stephan K. E., Fries P., and Moran R. J., "DCM for complex-valued data: Cross-spectra, coherence and phase-delays," *NeuroImage*, vol. 59, no. 1, pp. 439–455, 2012, https://doi.org/10.1016/j.neuroimage.2011.07.048 PMID: 21820062

44. Moran R. J., Stephan K. E., Seidenbecher T., Pape H. C., Dolan R. J., and Friston K. J., "Dynamic causal models of steady-state responses," *NeuroImage*, vol. 44, no. 3, pp. 796–811, 2009, https://doi.org/10.1016/j.neuroimage.2008.09.048 PMID: 19000769

45. Moran R., Pinotsis D. A., and Friston K., "Neural masses and fields in dynamic causal modelling," *Frontiers in Computational Neuroscience*, vol. 7, no. APR 2013, pp. 1–12, 2013, https://doi.org/10.3389/fncom.2013.00057 PMID: 23755005

46. Salin P. A. and Bullier J., "Corticocortical connections in the visual system: Structure and function," *Physiological Reviews*, vol. 75, no. 1, pp. 107–154, 1995, https://doi.org/10.1152/physrev.1995.75.1.107 PMID: 7831395

47. Sherman S. M. and Guillery R. W., "On the actions that one nerve cell can have on another: Distinguishing 'drivers' from 'modulators,'" *Proceedings of the National Academy of Sciences of the United States of America*, vol. 95, no. 12, pp. 7121–7126, 1998, https://doi.org/10.1073/pnas.95.12.7121 PMID: 9618549

48. Kiebel S. J., Garrido M. I., Moran R. J., and Friston K. J., "Dynamic causal modelling for EEG and MEG," *Cognitive Neurodynamics*, vol. 2, no. 2, pp. 121–136, 2008, https://doi.org/10.1007/s11571-008-9038-0 PMID: 19003479

49. Crone J. S., Ladurner G., Höller Y., Golaszewski S., Trinka E., and Kronbichler M., "Deactivation of the default mode network as a marker of impaired consciousness: An fmri study," *PLoS ONE*, vol. 6, no. 10, 2011, https://doi.org/10.1371/journal.pone.0026373 PMID: 22039473

50. Heine L. et al., "Resting state networks and consciousness Alterations of multiple resting state network connectivity in physiological, pharmacological, and pathological consciousness states," *Frontiers in Psychology*, vol. 3, no. AUG, pp. 1–12, 2012, https://doi.org/10.3389/fpsyg.2012.00295 PMID: 22969735

51. Lin P. et al., "Dynamic Default Mode Network across Different Brain States," *Scientific Reports*, vol. 7, no. March, pp. 1–13, 2017, https://doi.org/10.1038/srep46088 PMID: 28382944

52. Razi A. et al., "Large-scale DCMs for resting-state fMRI," *Network Neuroscience*, 2017, https://doi.org/10.1162/NETN_a_00015 PMID: 29400357

53. Xia M., Wang J., and He Y., "BrainNet Viewer: A Network Visualization Tool for Human Brain Connectomics.," *PLoS ONE*, vol. 8: e68910, 2013. https://doi.org/10.1371/journal.pone.0068910 PMID: 23861951

54. David O., Kiebel S. J., Harrison L. M., Mattout J., Kilner J. M., and Friston K. J., "Dynamic causal modeling of evoked responses in EEG and MEG," *NeuroImage*, vol. 30, no. 4, pp. 1255–1272, 2006, https://doi.org/10.1016/j.neuroimage.2005.10.045 PMID: 16473023

55. David O., Harrison L., and Friston K. J., "Modelling event-related responses in the brain," *NeuroImage*, vol. 25, no. 3, pp. 756–770, 2005, https://doi.org/10.1016/j.neuroimage.2004.12.030 PMID: 15808977

56. Jansen B. H. and Rit V. G., "Electroencephalogram and visual evoked potential generation in a mathematical model of coupled cortical columns," *Biological Cybernetics*, vol. 73, no. 4, pp. 357–366, 1995, https://doi.org/10.1007/BF00199471 PMID: 7578475

57. Friston K., Mattout J., Trujillo-Barreto N., Ashburner J., and Penny W., "Variational free energy and the Laplace approximation," *NeuroImage*, vol. 34, no. 1, pp. 220–234, 2007, https://doi.org/10.1016/j.neuroimage.2006.08.035 PMID: 17055746

58. Friston K. J. et al., "Bayesian model reduction and empirical Bayes for group (DCM) studies," *NeuroImage*, vol. 128, pp. 413–431, 2016, https://doi.org/10.1016/j.neuroimage.2015.11.015 PMID: 26569570

59. Friston K. and Penny W., "Post hoc Bayesian model selection," *NeuroImage*, vol. 56, no. 4, pp. 2089–2099, 2011, https://doi.org/10.1016/j.neuroimage.2011.03.062 PMID: 21459150

60. Rosa M. J., Friston K., and Penny W., "Post-hoc selection of dynamic causal models," *Journal of Neuroscience Methods*, vol. 208, no. 1, pp. 66–78, 2012, https://doi.org/10.1016/j.jneumeth.2012.04.013 PMID: 22561579

61. Ashburner J. et al., "SPM12 Manual The FIL Methods Group (and honorary members)," *Functional Imaging Laboratory*, pp. 475–1, 2017, https://doi.org/10.1111/j.1365-294X.2006.02813.x

62. Kiebel S. J., Garrido M. I., Moran R., Chen C.-C., and Friston K. J., "Dynamic causal modeling for EEG and MEG," *Human Brain Mapping*, vol. 30, no. 6, pp. 1866–1876, 2009, https://doi.org/10.1002/hbm.20775 PMID: 19360734

63. Koch C., Massimini M., Boly M., and Tononi G., "Neural correlates of consciousness: Progress and problems," *Nature Reviews Neuroscience*, vol. 17, no. 5, pp. 307–321, 2016, https://doi.org/10.1038/nrn.2016.22 PMID: 27094080

64. Siclari F., Baird B., Perogamvros L., Bernardi G., and Larocque J., "The neural correlates of dreaming," pp. 1–52, 2014, https://doi.org/10.1038/nn.4545 PMID: 28394322

65. Zeidman P. et al., "A guide to group effective connectivity analysis, part 2: Second level analysis with PEB," *NeuroImage*, vol. 200, no. May, pp. 12–25, 2019, https://doi.org/10.1016/j.neuroimage.2019.06.032 PMID: 31226492

66. Boly M. et al., "Connectivity Changes Underlying Spectral EEG Changes during Propofol-Induced Loss of Consciousness," *Journal of Neuroscience*, vol. 32, no. 20, pp. 7082–7090, 2012, https://doi.org/10.1523/JNEUROSCI.3769-11.2012 PMID: 22593076

67. Ihalainen R. et al., "How hot is the hot zone? Computational modelling clarifies the role of parietal and frontoparietal connectivity during anaesthetic-induced loss of consciousness," *NeuroImage*, vol. 231, no. January, p. 117841, 2021, https://doi.org/10.1016/j.neuroimage.2021.117841 PMID: 33577934

68. Moran R. J., Kiebel S. J., Stephan K. E., Reilly R. B., Daunizeau J., and Friston K. J., "A neural mass model of spectral responses in electrophysiology," *NeuroImage*, vol. 37, no. 3, pp. 706–720, 2007, https://doi.org/10.1016/j.neuroimage.2007.05.032 PMID: 17632015

69. Bastos A. M., Usrey W. M., Adams R. A., Mangun G. R., Fries P., and Friston K. J., "Canonical Microcircuits for Predictive Coding," *Neuron*, vol. 76, no. 4, pp. 695–711, 2012, https://doi.org/10.1016/j.neuron.2012.10.038 PMID: 23177956

70. Lee M. et al., "Connectivity differences between consciousness and unconsciousness in non-rapid eye movement sleep: a TMS–EEG study," *Scientific Reports*, vol. 9, no. 1, pp. 1–9, 2019, https://doi.org/10.1038/s41598-019-41274-2 PMID: 30914674

71. Alkire M. T., Hudetz A. G., and Tononi G., "Consciousness and Anesthesia," *Science*, vol. 322, no. 5903, pp. 867–880, 2008, https://doi.org/10.1126/science.1149213 PMID: 18988836

72. Wu X. et al., "Intrinsic functional connectivity patterns predict consciousness level and recovery outcome in acquired brain injury," *Journal of Neuroscience*, vol. 35, no. 37, pp. 12932–12946, 2015, https://doi.org/10.1523/JNEUROSCI.0415-15.2015 PMID: 26377477

73. Boveroux P. et al., "Breakdown of within- and between-network Resting State during Propofol-induced Loss of Consciousness," *Anesthesiology*, vol. 113, no. 5, pp. 1038–1053, 2010.

74. Vanhaudenhuyse A. et al., "Two Distinct Neuronal Networks Mediate the Awareness of Environment and of Self," *Journal of Cognitive Neuroscience*, vol. 23, no. 3, pp. 570–578, 2011. https://doi.org/10.1162/jocn.2010.21488 PMID: 20515407

75. Hohwy J., "The neural correlates of consciousness: New experimental approaches needed?," *Consciousness and Cognition*, vol. 18, no. 2, pp. 428–438, 2009, https://doi.org/10.1016/j.concog.2009.02.006 PMID: 19345590

76. Whitfield-Gabrieli S., Moran J. M., Nieto-Castañón A., Triantafyllou C., Saxe R., and Gabrieli J. D. E., "Associations and dissociations between default and self-reference networks in the human brain," *NeuroImage*, vol. 55, no. 1, pp. 225–232, 2011, https://doi.org/10.1016/j.neuroimage.2010.11.048 PMID: 21111832

77. Tshibanda L., Vanhaudenhuyse A., Galanaud D., Boly M., Laureys S., and Puybasset L., "Magnetic resonance spectroscopy and diffusion tensor imaging in coma survivors: promises and pitfalls," *Progress in Brain Research*, vol. 177, no. C, pp. 215–229, 2009, https://doi.org/10.1016/S0079-6123(09)17715-4 PMID: 19818904

78. Haufe S., Nikulin V., and Nolte G., "Identifying brain effective connectivity patterns from EEG: performance of Granger Causality, DTF, PDC and PSI on simulated data," *BMC Neuroscience*, 2011, https://doi.org/10.1186/1471-2202-12-S1-P141

79. Boly M. et al., "Response to Comment on 'Preserved Feedforward But Impaired Top-Down Processes in the Vegetative State,'" *Science*, vol. 334, no. 6060, p. 1203, 2011, https://doi.org/10.1126/science.1202043

80. Boly M. et al., "Intrinsic Brain Activity in Altered States of Consciousness: How Conscious Is the Default Mode of Brain Function?," *Annals of the New York Academy of Sciences*, vol. 1129, pp. 119–129, 2008, https://doi.org/10.1196/annals.1417.015 PMID: 18591474

81. Laureys S., "The neural correlate of (un)awareness: Lessons from the vegetative state," *Trends in Cognitive Sciences*, vol. 9, no. 12, pp. 556–559, 2005, https://doi.org/10.1016/j.tics.2005.10.010 PMID: 16271507

82. Greicius M. D., Kiviniemi V., Tervonen O., Vainionpää V., Reiss A. L., and Menon V., "Persistent Default- Mode Network Connectivity During Light Sedation," *Human brain mapping*, vol. 29, no. 7, pp. 839–847, 2008, https://doi.org/10.1002/hbm.20537 PMID: 18219620

83. Stamatakis E. A., Adapa R. M., Absalom A. R., and Menon D. K., "Changes in resting neural connectivity during propofol sedation," *PLoS ONE*, vol. 5, no. 12, 2010, https://doi.org/10.1371/journal.pone.0014224 PMID: 21151992

84. Horovitz S. G. et al., "Decoupling of the brain's default mode network during deep sleep," *Proceedings of the National Academy of Sciences*, vol. 106, no. 27, pp. 11376–11381, 2009, https://doi.org/10.1073/pnas.0901435106 PMID: 19549821

85. Newcombe V. et al., "Aetiological differences in neuroanatomy of the vegetative state: Insights from diffusion tensor imaging and functional implications," *Journal of Neurology, Neurosurgery and Psychiatry*, vol. 81, no. 5, pp. 552–561, 2010, https://doi.org/10.1136/jnnp.2009.196246 PMID: 20460593

86. Baars B. J., "A Cognitive Theory of Consciousness," NY: Cambridge University Press, 1988.

87. Baars B. J., "In the theatre of consciousness. Global Workspace Theory, a rigorous scientific theory of consciousness," *Journal of Consciousness Studies*, vol. 4, no. 4, pp. 292–309, 1997, https://doi.org/10.1093/acprof:oso/9780195102659.001.1

88. Dehaene S., Changeux J.-P., and Naccache L., "The Global Neuronal Workspace Model of Conscious Access: From Neuronal Architectures to Clinical Applications," in *Characterizing Consciousness*: *From Cognition to the Clinic*?. *Research and Perspectives in Neurosciences*., vol. 18, Dehaene S. and Christen Y., Eds., Springer, Berlin, Heidelberg., 2011, pp. 55–84. https://doi.org/10.1007/978-3-642-18015-6

89. Mashour G. A., Roelfsema P., Changeux J. P., and Dehaene S., "Conscious Processing and the Global Neuronal Workspace Hypothesis," *Neuron*, vol. 105, no. 5, pp. 776–798, 2020, https://doi.org/10.1016/j.neuron.2020.01.026 PMID: 32135090

90. Di Perri C. et al., "Limbic hyperconnectivity in the vegetative state," *Neurology*, vol. 81, no. 16, pp. 1417–1424, Oct. 2013, https://doi.org/10.1212/WNL.0b013e3182a43b78 PMID: 24049132

91. Di Perri C. et al., "Multifaceted brain networks reconfiguration in disorders of consciousness uncovered by co-activation patterns," *Human Brain Mapping*, vol. 39, no. 1, pp. 89–103, 2018, https://doi.org/10.1002/hbm.23826 PMID: 29024197

92. Demertzi A., Soddu A., and Laureys S., "Consciousness supporting networks," *Current Opinion in Neurobiology*, vol. 23, no. 2, pp. 239–244, Apr. 2013, https://doi.org/10.1016/j.conb.2012.12.003 PMID: 23273731

93. Fedorenko E., Hsieh P.-J., Nieto-Castañón A., Whitfield-Gabrieli S., and Kanwisher N., "New Method for fMRI Investigations of Language: Defining ROIs Functionally in Individual Subjects," *Journal of Neurophysiology*, vol. 104, no. 2, pp. 1177–1194, Aug. 2010, https://doi.org/10.1152/jn.00032.2010 PMID: 20410363

94. Fedorenko E. and Thompson-Schill S. L., "Reworking the language network," *Trends in Cognitive Sciences*, vol. 18, no. 3, pp. 120–126, Mar. 2014, https://doi.org/10.1016/j.tics.2013.12.006 PMID: 24440115

95. Mineroff Z., Blank I. A., Mahowald K., and Fedorenko E., "A robust dissociation among the language, multiple demand, and default mode networks: Evidence from inter-region correlations in effect size," *Neuropsychologia*, vol. 119, pp. 501–511, Oct. 2018, https://doi.org/10.1016/j.neuropsychologia.2018.09.011 PMID: 30243926